

Dalton Transactions

Accepted Manuscript



This is an *Accepted Manuscript*, which has been through the Royal Society of Chemistry peer review process and has been accepted for publication.

Accepted Manuscripts are published online shortly after acceptance, before technical editing, formatting and proof reading. Using this free service, authors can make their results available to the community, in citable form, before we publish the edited article. We will replace this *Accepted Manuscript* with the edited and formatted *Advance Article* as soon as it is available.

You can find more information about *Accepted Manuscripts* in the [Information for Authors](#).

Please note that technical editing may introduce minor changes to the text and/or graphics, which may alter content. The journal's standard [Terms & Conditions](#) and the [Ethical guidelines](#) still apply. In no event shall the Royal Society of Chemistry be held responsible for any errors or omissions in this *Accepted Manuscript* or any consequences arising from the use of any information it contains.

A tricarboxylated PtCl(terpyridine) derivative exhibiting pH-dependent photocatalytic activity for H₂ evolution from water

Kosei Yamauchi,^{*ab} and Ken Sakai^{*abc}

^aDepartment of Chemistry, Faculty of Sciences, Kyushu University, 6-10-1 Hakozaki, Higashi-ku, Fukuoka 812-8581, Japan. E-mail: kyamauchi@chem.kyushu-univ.jp, ksakai@chem.kyushu-univ.jp

^bInternational Institute for Carbon-Neutral Energy Research (WPI-I2CNER), Kyushu University, Motooka 744, Nishi-ku, Fukuoka 819-0395, Japan.

^cCenter for Molecular Systems (CMS), Kyushu University, Motooka 744, Nishi-ku, Fukuoka 819-0395, Japan.

Abstract

The first negatively charged PtCl(tpy) (tpy = 2,2':6',2''-terpyridine) derivative, formulated as $\text{Na}_2[\text{PtCl}(\text{tctpy})]\cdot 5\text{H}_2\text{O}$ (tctpy = 2,2':6',2''-terpyridine-4,4',4''-tricarboxylate), was prepared, characterized, and investigated in detail for its activity as a single-component photocatalyst which drives water reduction to H_2 in the presence of a sacrificial electron donor (EDTA). This compound was confirmed to exist in its fully deprotonated form $[\text{PtCl}(\text{tctpy})]^{2-}$ in aqueous media at $\text{pH} > 4.4$. In spite of its dianionic character, $[\text{PtCl}(\text{tctpy})]^{2-}$ was found to form a specific adduct with anionic EDTA (i.e., YH_2^{2-} and YH^{3-} , where YH_4 is a fully protonated form of EDTA), enabling reductive quenching of the triplet metal-to-ligand charge transfer excited state within the adduct leading to subsequent electron transfer steps correlated with Pt(II)-catalyzed H_2 evolution from water. Electrochemical studies also reveal that the compound exhibits a unique pH-dependent first reduction (i.e., tctpy-centered reduction), leading to our realization of the first example of a Pt(II)-based molecular system photocatalyzing H_2 evolution reaction accompanied by a ligand-based proton-coupled electron transfer (PCET) process.

Introduction

Solar-driven water splitting ($2\text{H}_2\text{O} + 4h\nu \rightarrow 2\text{H}_2 + \text{O}_2$) is now considered as one of the promising candidates to solve the problems arising from shortage of fossil fuels and global warming due to continued emission of CO_2 .¹⁻⁴ As part of our efforts to develop molecule-based artificial photosynthetic devices for enabling photocatalytic water oxidation and reduction, continuous efforts have been made to examine the hydrogen evolution reaction (HER) promoted by Pt(II)-based homogeneous catalysts.⁴ Earlier studies relied on the use of a well-known three-component photosystem consisting of EDTA, $[\text{Ru}(\text{bpy})_3]^{2+}$ (photosensitizer; bpy = 2,2'-bipyridine), and methylviologen (MV^{2+} ; electron relay), in which photochemically generated $\text{MV}^{+\bullet}$ serves as a reducing equivalent to drive water reduction based on the reaction: $2\text{MV}^{+\bullet} + 2\text{H}^+ \rightarrow 2\text{MV}^{2+} + \text{H}_2$ (see Scheme 1).⁵ Importantly, the thermodynamic driving force (DF) for this reaction at pH 5.0 is only 150 meV.^{5c,6} In spite of such a small DF, various platinum(II) complexes have been confirmed to accelerate $\text{MV}^{+\bullet}$ -driven HER under these conditions.⁵ The highly active character of platinum(II) complexes has been suggested to arise from their characteristic pathway for the catalysis of HER, which proceeds via rate-determining PCET steps leading to hydridoplatinum(III) intermediates: $\text{Pt}^{\text{II}} + \text{H}^+ + \text{e}^- \rightarrow \text{Pt}^{\text{III}}\text{-H}$.^{5d} Our DFT calculations revealed that the initial PCET step is an uphill process but two possible subsequent steps are sufficiently downhill processes, i.e., unimolecular and bimolecular H_2 evolution steps; $\text{Pt}^{\text{III}}\text{-H} + \text{H}^+ + \text{e}^- \rightarrow \text{Pt}^{\text{II}} + \text{H}_2$ and

$2\text{Pt}^{\text{III}}\text{-H} \rightarrow 2\text{Pt}^{\text{II}} + \text{H}_2$.^{5d} We also reported rare examples of Rh^{II} - and Co^{II} -catalyzed HER,^{7,8} which proceeds via an analogous PCET step affording a hydride intermediate without generating lower valent intermediates often considered to take part in the catalytic paths for some well-known H_2 -evolving catalysts having a Co or Ni center.^{1b,1g,9,10} These Co- and Ni-based molecular catalysts have been considered to afford hydride intermediates via oxidative addition of proton to a lower valence intermediate; e.g., $\text{Co}^{\text{II}} + \text{e}^- \rightarrow \text{Co}^{\text{I}}$ followed by $\text{Co}^{\text{I}} + \text{H}^+ \rightarrow \text{Co}^{\text{III}}\text{-H}$.

We also attempted to fabricate photo-hydrogen-evolving molecular devices (PHEMDs) that can promote both photo-driven electron transfer (ET) and Pt(II)-catalyzed HER within a single molecular motif. The RuPt^{2+} derivatives depicted in Scheme 2 were shown to be the first important series of PHEMDs.^{4b,11,12} For this family, the photo-hydrogen-evolving (PHE) activity was examined by changing the substituent R, which resulted in our conclusion that the DF for the intramolecular ET governs the apparent photocatalytic activity of PHEMDs.^{12b} On the other hand, quite simple mononuclear platinum(II) complexes having a bpy or tpy derivative were also proven to serve as PHEMDs.¹³ For these systems, the so-called ³MLCT (triplet metal-to-ligand charge transfer) or ³MMLCT (triplet metal-metal-to-ligand charge transfer) excited state, derived from the $\text{PtCl}_2(\text{bpy})$, $\text{PtCl}(\text{tpy})$, or $[\text{PtCl}(\text{tpy})]_2$ dimer chromophore, is considered to participate in the initial photo-driven ET step (i.e., reductive quenching of the triplet by EDTA). Due to the relatively short lifetimes of these triplet states

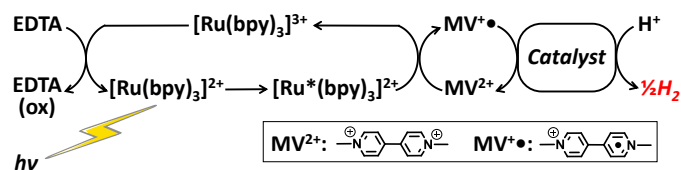
in aqueous media at room temperature,¹⁴ ground-state adduct formation between the cationic PHEMDs and dianionic EDTA (i.e., YH_2^{2-} ; 93% in abundance at pH = 5.0) has been found to play a key role in affording a reductively quenched product according to Scheme 3.

Insert Scheme 3

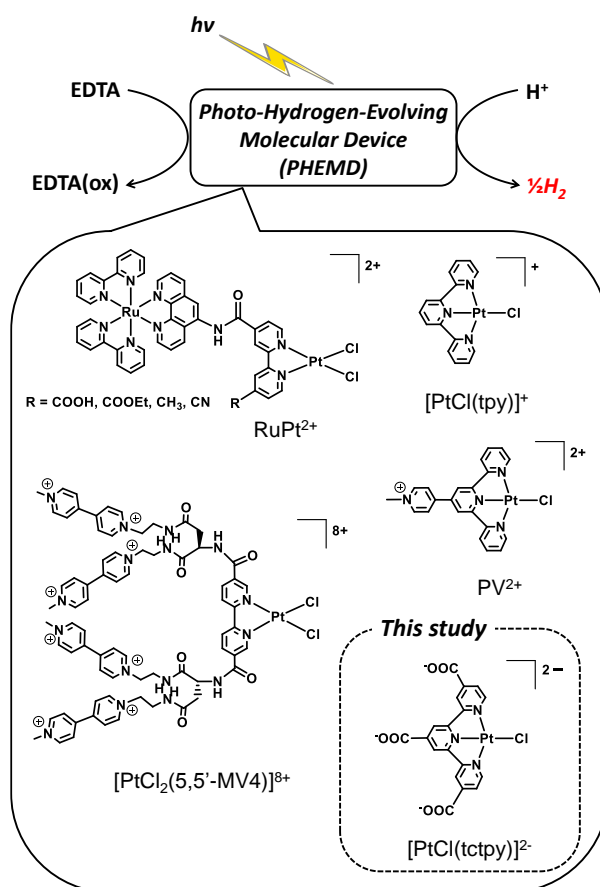
These studies revealed that the HER photocatalyzed by either PV^{2+} or $[\text{PtCl}_2(5,5'\text{-MV}_4)]^{8+}$ (see Scheme 2) proceeds based on the following two-step excitation (Z-Scheme; see Scheme 4).^{13c,d}

Insert Scheme 4

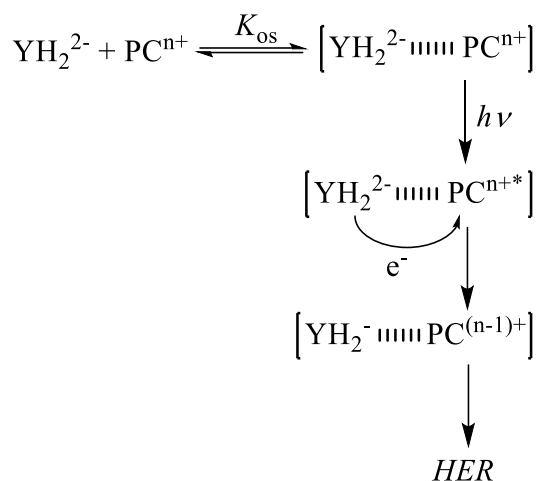
As mentioned above, all the PHEMDs examined so far possess a positive charge enabling ion-pair formation with dianionic YH_2^{2-} . In the present study, we focus for the first time on a negatively charged $\text{PtCl}(\text{tpty})$ derivative having three carboxylate units ($[\text{PtCl}(\text{tctpy})]^{2-}$; Scheme 2). This compound was originally designed to avoid deposition of a neutral one-electron-reduced product $\text{PtCl}(\text{tpty}^{\bullet-})$ while we were examining the photocatalysis of $[\text{PtCl}(\text{tpty})]^+$ in further detail, but later turned out to provide additional important insights into this series, as reported in this study. An important realization is that such a negatively charged system can also afford a specific adduct with anionic EDTA and does show PHE activity. Moreover, this study clarifies intriguing pH-dependent redox properties of $[\text{PtCl}(\text{tctpy})]^{2-}$ due to the increased basicity of the carboxylates upon its one-electron reduction into $[\text{PtCl}(\text{tctpy}^{\bullet-})]^{3-}$.



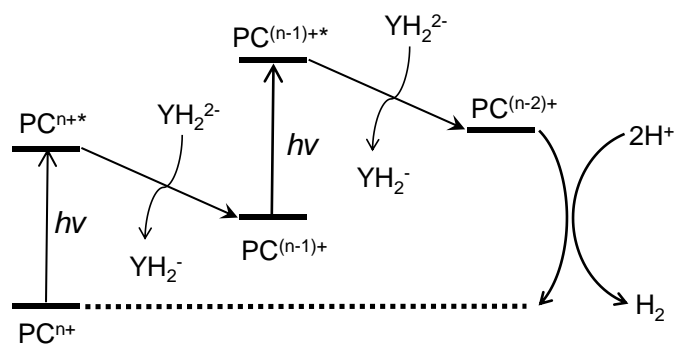
Scheme 1 A three-component system driving photochemical H_2 production from water.



Scheme 2 Pt(II)-based PHEMDs promoting photo-driven HER.



Scheme 3 Ion-pair adduct formation between a cationic PHEMD and an anionic EDTA, where PC^{n+} is equivalent to PHEMD.



Scheme 4 Z-scheme photosynthesis of PHEMD, where PC^{n+} denotes PHEMD.

Results and discussion

Spectroscopic and structural properties

First, the absorption spectrum of $\text{Na}_2[\text{PtCl}(\text{tctpy})]$ in aqueous media was found to be sensitive to the Cl^- concentration (Fig. S1), indicating that the hydrolysis equilibrium in eq. 1 is shifted to the hydrolyzed form at lower Cl^- concentrations.



From the Cl^- concentration dependence of absorbance data (Fig. S1), it is clear that the concentration of the hydrolyzed species becomes negligible at Cl^- concentrations above 0.075 M. To satisfy this requirement, all the experiments described below were conducted in the presence of 0.1 M NaCl. The $[\text{PtCl}(\text{tctpy})]^{2-}$ concentration dependence of absorbance data reveals that Beer's law is obeyed at concentrations below 1.0 mM (Fig. S2), indicating dimerization of $[\text{PtCl}(\text{tctpy})]^{2-}$ in aqueous media is negligible under these conditions. This is in sharp contrast with the dimerization behaviour of $[\text{PtCl}(\text{tpy})]^+$, which was reported to have a dimerization constant of $K_d = (4 \pm 2) \times 10^3 \text{ M}^{-1}$.¹⁵ Perhaps, dimerization of $[\text{PtCl}(\text{tctpy})]^{2-}$ is considerably hindered due to the stronger electrostatic repulsion between these dianionic species. Contribution of protonated species (i.e., $[\text{PtCl}(\text{tctpyH})]^-$, $\text{PtCl}(\text{tctpyH}_2)$, and $[\text{PtCl}(\text{tctpyH}_3)]^+$) is negligible and the triply deprotonated species is judged to be the major species in solution in the pH range 4.4–7.4, since no spectral change is observed under these pH conditions (see Fig. S3). Since precipitate starts to form at pH below ca. 4.2, the singly or

doubly protonated species must be formed to cause deposition of a solid around this pH. The ¹MLCT band of [PtCl(tctpy)]²⁻ is ca. 20 nm red-shifted relative to that of [PtCl(tpy)]⁺ (see Fig. 1A), presumably due to the electron-withdrawing effects of three carboxylate groups on the terpyridyl moiety.

Neither aqueous nor methanolic solutions of [PtCl(tctpy)]²⁻ exhibit emission at room temperature even under degassed conditions, probably due to efficient nonradiative decay via low-lying d-d excited states or solvent interactions at the open coordination sites.¹⁴ Whereas, [PtCl(tctpy)]²⁻ exhibits green emission in a methanol-ethanol-dmf (MED; 4:4:1, where dmf = *N,N*-dimethylformamide) mixture under frozen glass conditions at 77 K (Fig. 2A). Vibrationally structured bands appear at 488, 522, and 562 nm, where the spacing between the 0–0 and 0–1 transitions is 1300 cm⁻¹. These results, together with the long emission lifetime (10.6 μs; see also Fig. 2B) and a relatively large Stokes shift (ca. 100 nm), clearly indicate that the emission arises from the triplet excited state. This encourages us to consider that this ³MLCT excited state contributes to reductive quenching of the photoexcited [PtCl(tctpy)]²⁻ by EDTA, as illustrated in Scheme 3.

To better understand the electronic properties of [PtCl(tctpy)]²⁻, the structure of [PtCl(tctpy)]²⁻ in aqueous media was calculated using density functional theory (DFT) calculation at the M06 level. As shown in Fig. 3, the optimized structure has C_{2v} symmetry with all atoms coplanar (see also Table S1). The bond distances and angles within the

coordination sphere can be compared with those of $[\text{PtCl}(\text{tpy})]^+$ (Table S2), optimized using the same level of calculation (Fig. 3; see also Table S3). All Pt–N(pyridyl) bond distances in $[\text{PtCl}(\text{tctpy})]^{2-}$ are 0.008–0.014 Å shorter than the corresponding bond distances in $[\text{PtCl}(\text{tpy})]^+$ (see Fig. 3), reflecting the stronger electrostatic attraction between the Pt ion and the anionic tctpy^{3-} ligand. Due to this feature, the trans influence originated by the central Pt–N(pyridyl) bond is stronger in $[\text{PtCl}(\text{tctpy})]^{2-}$ relative to $[\text{PtCl}(\text{tpy})]^+$, which is evidenced by the slightly longer Pt–Cl bond in $[\text{PtCl}(\text{tctpy})]^{2-}$ compared to that in $[\text{PtCl}(\text{tpy})]^+$ (see Fig. 3). This feature is also relevant to the above-mentioned chloride dissociation (i.e., hydrolysis) in eq. 1). On the other hand, a simulated absorption spectrum of $[\text{PtCl}(\text{tctpy})]^{2-}$ based on TD-DFT results is somewhat consistent with the observed spectrum (Figs. 1A,B). The lowest-energy band at 385.98 nm ($f = 0.040$) corresponds to a transition from HOMO–3 [$\text{dxz}(\text{Pt})$, $\pi(\text{tctpy})$, and $\text{pz}(\text{Cl})$] to LUMO [$\pi^*(\text{tctpy})$] (see Table S4). This is characterized as a mixed MLCT transition with significant contributions of ligand-centered (LC) and halide-to-ligand charge transfer (XLCT) transitions.

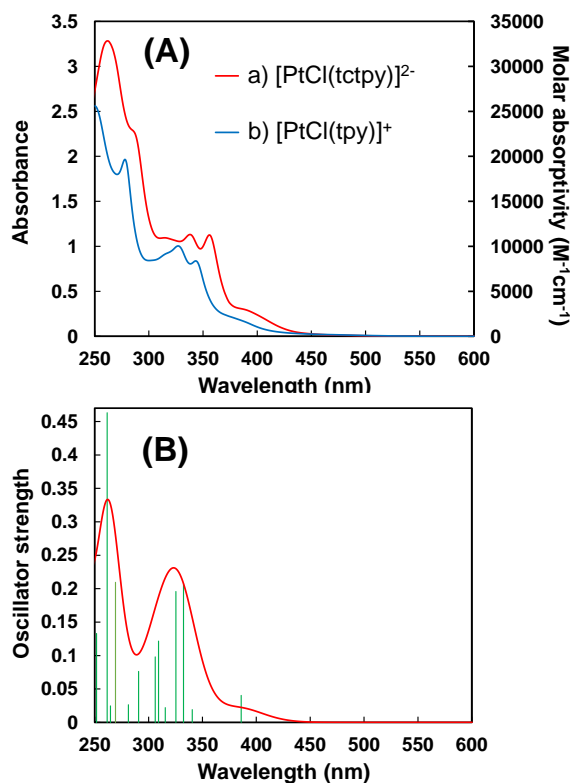


Fig. 1 (A) UV-vis absorption spectra of 0.1 mM a) $\text{Na}_2[\text{PtCl}(\text{tctpy})]\cdot 5\text{H}_2\text{O}$ and b) $[\text{PtCl}(\text{tpy})]\text{Cl}\cdot 2\text{H}_2\text{O}$ in an aqueous 0.1 M NaCl solution at 20 °C in air. (B) Calculated absorption spectra of $[\text{PtCl}(\text{tctpy})]^{2-}$ (red). The singlet excitations, simulated with Gaussian function, are shown as vertical bars (green) with heights equal to the oscillator strength.

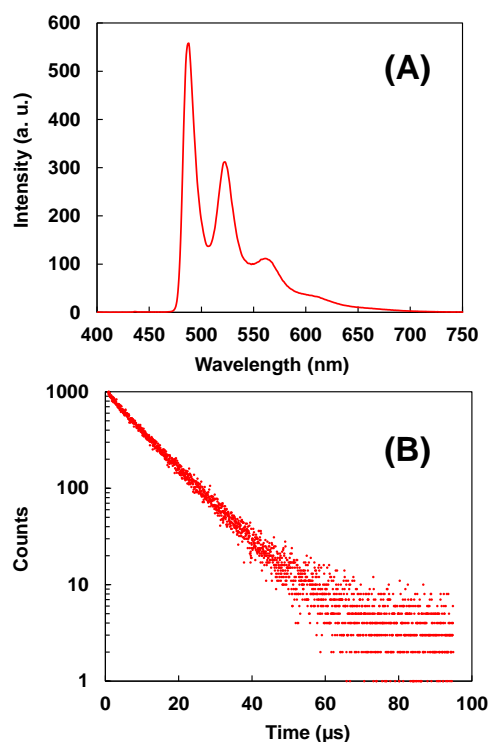


Fig. 2 (A) Emission spectra ($\lambda_{\text{ex}} = 374 \text{ nm}$) and (B) emission decay profiles (monitored at 487 nm) of $[\text{PtCl}(\text{tctpy})]^{2-}$ in a frozen glass state (MED) at 77 K in air. An excess of benzo-15-crown-5 (10 equiv.) was added to this solution in order to solubilize $\text{Na}_2[\text{PtCl}(\text{tctpy})]$ in MED.

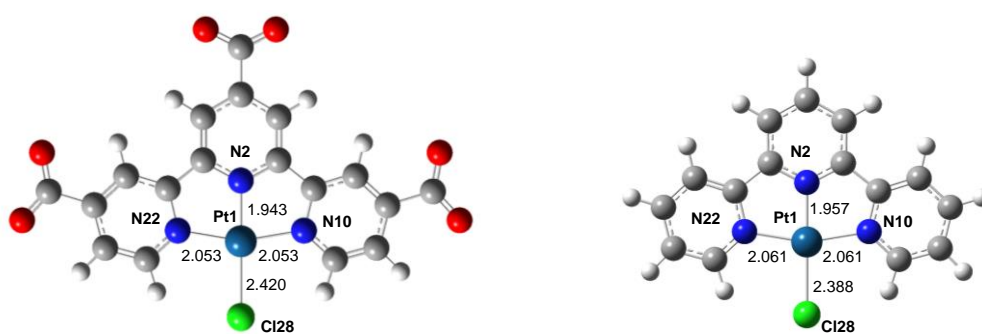


Fig. 3 The geometries of $[\text{PtCl}(\text{tctpy})]^{2-}$ (left) and $[\text{PtCl}(\text{tpy})]^+$ (right) in their water-solvated models (PCM) optimized at the M06 level of DFT using the LanL2DZ basis set for Pt and the 6-31+G(d,p) basis set for H, C, N, O, and Cl.

Electrochemistry

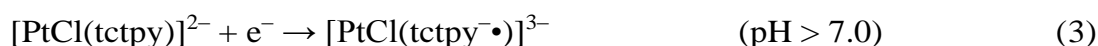
In order to solubilize $\text{Na}_2[\text{PtCl}(\text{tctpy})]$ in dry dmf, a slight excess of dibenzo-18-crown-6 (dbc) was added to the solution prepared for electrochemical studies (see Fig. 4 for detail). In other words, we may formally suppose that the solution was prepared by dissolving $[\text{Na}(\text{dbc})]_2[\text{PtCl}(\text{tctpy})]$ in dmf. As shown in Fig. 4, $[\text{PtCl}(\text{tctpy})]^{2-}$ displays two reversible reduction waves at -0.98 ($E_{\text{red},1}$) and -1.50 ($E_{\text{red},2}$) V vs. SCE, which are quite comparable to the values of -0.93 and -1.49 V previously reported for $[\text{PtCl}(\text{tpy})]^+$.¹⁶ The electrochemical parameters provide an estimate for the comproportionation constant ($K_c = e^{(F/RT) \cdot \Delta E}$, $\Delta E = E_{\text{red},1} - E_{\text{red},2}$) for eq. 2, where F is a Faraday constant, R is a gas constant, and T is an absolute temperature (K).



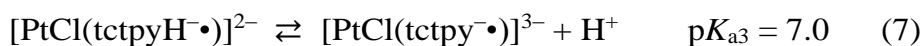
The value is estimated as $K_c = 6.2 \times 10^8$, indicating that the equilibrium is largely shifted to the right, and thereby formation of the doubly reduced species in dmf through disproportionation of the one-electron-reduced species is negligible.

The first reduction potential ($E_{\text{red},1}$) of $[\text{PtCl}(\text{tctpy})]^{2-}$ in aqueous media can be observed using square wave voltammetric technique. Interestingly, $E_{\text{red},1}$ is found to be highly sensitive to pH (Fig. S4) and affords a Pourbaix diagram showing somewhat complicated pH-dependent behaviours (Fig. 5A). The first reduction is observed to occur at a constant potential above pH = 7.0, indicating that this reduction is not coupled with any proton

transfer process, leading to our assignment in eq. 3. On the other hand, the slope for the first reduction as a function of pH is estimated as -0.059 V/pH for $\text{pH} = 5.1-7.0$ and -0.132 V/pH for $\text{pH} = 4.5-5.1$. These results indicate that one-electron reduction of $[\text{PtCl}(\text{tctpy})]^{2-}$ at $\text{pH} = 5.1-7.0$ is coupled with a single protonation process (eq. 4), while the reduction at $\text{pH} = 4.5-5.1$ is coupled with a double protonation process (eq. 5).



These results reveal that the pK_a values of the singly reduced species ($[\text{PtCl}(\text{tctpyH}_n^{-\bullet})]^{(3-n)-}$; $n = 1,2,3$) are significantly higher than those of the initial non-reduced species ($[\text{PtCl}(\text{tctpyH}_n)]^{(2-n)-}$; $n = 1,2,3$). Consequently, the values are estimated as $\text{pK}_{a2} = 5.1$ and $\text{pK}_{a3} = 7.0$ for the singly reduced species (eqs. 6,7), where pK_{a1} could not be determined under these conditions.

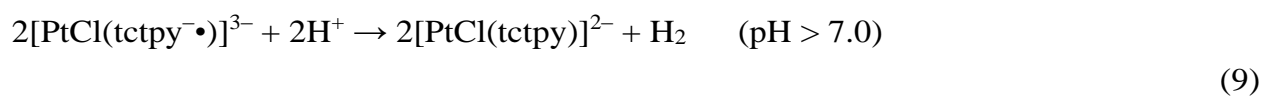


Note that the standard electrode potential for HER is defined by eq. 8 (see also Fig. 5A).

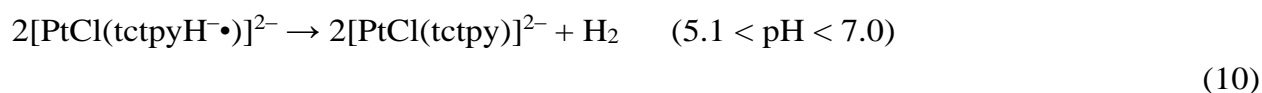
$$E_{1/2}(2\text{H}^{+}/\text{H}_2) = -0.241 - 0.059 \text{ pH (V vs. SCE)} \quad (8)$$

Since the formal first reduction potential of $[\text{PtCl}(\text{tctpy})]^{2-}$ is constant above $\text{pH} = 7.0$, the DF for the thermal HER driven by the one-electron-reduced form of $[\text{PtCl}(\text{tctpy})]^{2-}$ decreases at

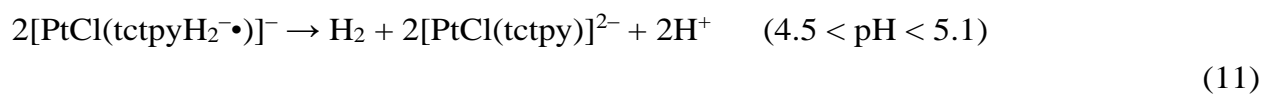
higher pH as given in eq. 9 (see also Fig. 5B). Importantly, the DF for the HER at pH = 5.1-7.0 is insensitive to pH and remains constant (0.15 eV) as given in eq. 10 (Fig. 5B). On the other hand, the first reduction potential of $[\text{PtCl}(\text{tctpy})]^{2-}$ is much more sensitive to pH with the highest slope at pH = 4.5-5.1. Because of this feature, the DF for HER decreases with decreasing pH in this pH range (see eq. 11 and Fig. 5B).



$$\text{DF} = 0.562 - 0.059 \text{ pH (eV)} \quad (\text{e.g. DF} = 0.120 \text{ eV at pH 7.5})$$



$$\text{DF} = 0.150 \text{ (eV)}$$



$$\text{DF} = 0.073 \text{ pH} - 0.225 \text{ (eV)} \quad (\text{e.g. DF} = 0.125 \text{ eV at pH 4.8})$$

In summary, the highest DF (150 meV) for the thermal HER driven by the one-electron-reduced species $[\text{PtCl}(\text{tctpyH}^{-\bullet})]^{2-}$ is achieved in the pH range 5.1-7.0. This is the first example of a Pt(II)-based H_2 -evolving catalyst which exhibits pH-independent DF for HER owing to the PCET character of the redox couple correlated with HER.

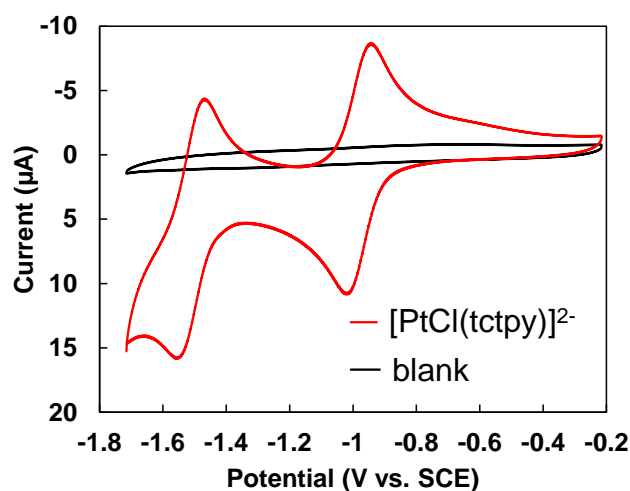


Fig. 4 A cyclic voltammogram of $[\text{PtCl}(\text{tctpy})]^{2-}$ (0.5 mM) in dmf containing 0.1 M TBAP (tetra(n-butyl)ammonium perchlorate) as a supporting electrolyte, recorded at a scan rate of 100 mV/s under Ar in the dark at room temperature. In this experiment, a slight excess of dibenzo-18-crown-6 (4 equiv.) together with $\text{Na}_2[\text{PtCl}(\text{tctpy})]\cdot 5\text{H}_2\text{O}$ was dissolved in a small amount of methanol, followed by adding dmf. Most of the methanol is considered to be removed by purging with Ar before scanning.

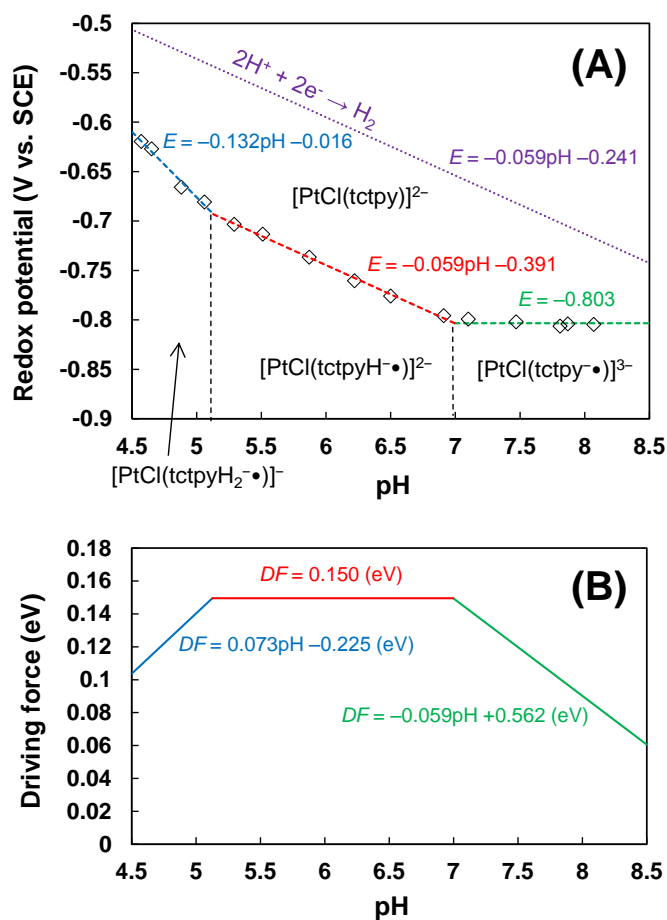


Fig. 5 (A) Plot of the first reduction potential ($E_{\text{red},1}$) of $[\text{PtCl}(\text{tctpy})]^{2-}$ as a function of pH (Pourbaix diagram), where potentials were determined by observing the square wave voltammograms of the complex in aqueous media at various pH conditions. See Fig. S4 for details. (B) The DF for the thermal HER driven by the singly reduced species of $[\text{PtCl}(\text{tctpy})]^{2-}$ as a function of pH.

Photocatalytic H₂ production from water

The PHE activity of $[\text{PtCl}(\text{tctpy})]^{2-}$ was first evaluated by visible light irradiation of aqueous solutions of the complex at a constant pH (0.1 M acetate buffer, pH = 5.0) in the presence of 0.1 M NaCl and 30 mM EDTA. As shown in Fig. 6a, $[\text{PtCl}(\text{tctpy})]^{2-}$ was confirmed to serve as a PHEMD. The TON (2.4 at 12 h) is lower than that recently reported for the multiviologen-tethered $\text{PtCl}_2(\text{bpy})$ systems (e.g., TON = 27 at 12 h for $[\text{PtCl}_2(5,5' \text{-MV4})]^{8+}$),^{13d} but is comparable to that reported for one of the RuPt^{2+} derivatives with R = COOH (TON = 2.4 at 10 h), which was reported as the first active model of PHEMD.¹¹ Importantly, degradation of $[\text{PtCl}(\text{tctpy})]^{2-}$ during the photocatalysis is suppressed under these conditions as seen for the H₂ evolution curve in Fig. 6a, whereas $[\text{PtCl}(\text{tpy})]^+$ was confirmed to lose activity within an hour due to the replacement of the chloride ligand by a coexisting donor ligand in solution.^{13a} On the other hand, an unexpected result was given in a control experiment carried out for $[\text{PtCl}(\text{tpy})]^+$ under the conditions adopted in the above experiments. As depicted in Fig. 6b, no H₂ evolution occurs despite that our previous two reports showed that this complex is active as a PHEMD in the absence of any chloride salt at identical pH; one was examined using a different buffer (MES; 2-(N-morpholino)ethanesulfonic acid)^{13a} while the other using the same acetate buffer.^{13b} The loss in the PHE activity of $[\text{PtCl}(\text{tpy})]^+$ in the presence of NaCl (0.1 M) is attributable to the deposition of one-electron-reduced species $\text{PtCl}(\text{tpy}^{\bullet-})$ as blue precipitate (see Fig. S5). The

manner how deposition proceeds could be more quantitatively observed by using dynamic light scattering (DLS) technique. As shown in Fig. 7a, within a minute after starting photoirradiation, an abrupt increase is seen in the light scattering intensity measured for the EDTA/[PtCl(tpy)]⁺ system in the presence of 0.1 M NaCl. Quite similar behaviour was observed spectrophotometrically (Figs. S6A,B), in which growth of new broad low-energy bands in the visible and near infrared region can be seen. Moreover, these absorption features are also given by merely mixing [PtCl(tpy)]⁺ with MV^{+•}, generated in situ by controlled potential electrolysis of MV²⁺ (Fig. S6C). We conclude that these bands originate from absorption by radical species within the heterogeneous particles (ca. 10 μm at 10 min via DLS), since the solution became colorless after the suspension was left for about an hour to let the particles deposited on the bottom of the measurement cell. These results indicate that an insoluble neutral complex PtCl(tpy^{-•}) is formed through reductive quenching of the photoexcited state of [PtCl(tpy)]⁺ ([PtCl(tpy)]^{+*}) by EDTA to inactivate all the relevant PHE processes.

In contrast, the increase in the light scattering intensity during the photocatalysis of [PtCl(tctpy)]²⁻ is negligible over 7 h (Fig. 7b), revealing that all intermediate species generated during the photolysis, such as the one-electron-reduced species of [PtCl(tctpy)]²⁻ (i.e., [PtCl(tctpyH_n^{-•})]⁽³⁻ⁿ⁾⁻; the major species adopts n = 2 at pH = 5.0: see above), are well soluble in aqueous media (see Fig. 7b). Furthermore, the lack of any particle formation also

evidences that colloidal platinum formation during the photolysis of $[\text{PtCl}(\text{tctpy})]^{2-}$ is negligible, which strongly supports the homogeneous character of the present photocatalysis.

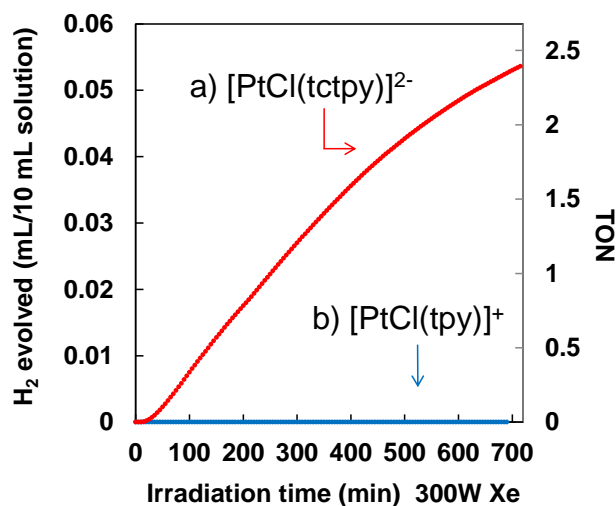


Fig. 6 Photochemical H_2 production from an aqueous acetate buffer solution (0.1 M, pH = 5.0; 10 mL) containing EDTA \cdot 2Na (30 mM) and 0.1 M NaCl in the presence of a) 0.1 mM $\text{Na}_2[\text{PtCl}(\text{tctpy})]\cdot 5\text{H}_2\text{O}$ or b) $[\text{PtCl}(\text{tpy})]\text{Cl}\cdot 2\text{H}_2\text{O}$ at 20 °C under Ar atmosphere.

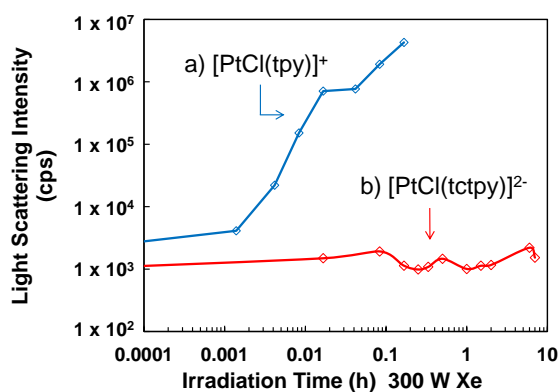


Fig. 7 In situ DLS measurements during the photolysis (300 W Xe lamp, 400-800 nm) of an aqueous acetate buffer solution (0.1 M, pH = 5.0) containing $\text{Na}_2[\text{YH}_2]$ (30 mM) and 0.1 M NaCl in the presence of a) 0.1 mM $\text{Na}_2[\text{PtCl}(\text{tctpy})]\cdot 5\text{H}_2\text{O}$ or b) 0.1 mM $[\text{PtCl}(\text{tpy})]\text{Cl}\cdot 2\text{H}_2\text{O}$ at 20 °C under Ar atmosphere.

pH dependence of photodriven HER by $[\text{PtCl}(\text{tctpy})]^{2-}$

As discussed above, $[\text{PtCl}(\text{tctpy})]^{2-}$ is a unique example for which PHE activity can be examined as a function of pH because of its protonation at the three carboxylate groups of the reduced species. Fig. 8A shows the H_2 evolution curves observed at various pH conditions. In these experiments, pH values were adjusted by changing the mixing ratio of $\text{Na}_2[\text{YH}_2]$ and $\text{Na}_3[\text{YH}]$ by adopting a constant total EDTA concentration ($[\text{Y}]_{\text{t}} = [\text{YH}^{3-}] + [\text{YH}_2^{2-}] = 30$ mM). The pH dependence of the maximum H_2 evolution rate estimated from these data provides a unique volcano-like diagram depicted in Fig. 8B. The maximum rate occurs at $\text{pH} = 6.2$, which also coincides with the pH at which the concentration of YH_2^{2-} and YH^{3-} are equal (Fig. 8C). Importantly, this pH lies within the pH range where the highest/constant DF is applied according to eq. 10 (see also Fig. 5B). At this pH, $\text{TON} = 4.6$ (12 h) is achieved when the $[\text{PtCl}(\text{tctpy})]^{2-}$ concentration is 0.4 mM (see Fig. S7).

In order to better understand the behaviours of chemical species in solution, the reactions during photocatalysis were examined spectrophotometrically at three different pH conditions. As shown in Figs. 9A-C, growth of broad visible and near infrared absorption bands is observed at all pH conditions. For all cases, the absorption band gradually decays at the prolonged photolysis stage after the final recording time in these figures; the final spectrum at each pH was recorded when the maximum concentration is given for the reduced species during the course of photolysis. These bands are attributable to a one-electron-reduced

species. The pH-dependent character observed in these spectral data clearly reflects the shifts of protonation equilibria for $[\text{PtCl}(\text{tctpyH}_n\cdot)]^{(3-n)-}$ (eqs. 6,7). Strictly speaking, both $[\text{PtCl}(\text{tctpyH}^-\cdot)]^{2-}$ and $[\text{PtCl}(\text{tctpyH}_2^-\cdot)]^-$ are considered to possess two different protonation forms (see Fig. 10). As a consequence, five species must be thus taken into consideration, including a non-protonated form, as shown in Fig. 10. As a result, five spectral features can be simulated based on the results of TD-DFT calculations (Fig. 10). Particularly, the simulated spectrum of the non-protonated species well resembles that observed at pH = 7.5 where the relative abundance of $[\text{PtCl}(\text{tctpy}^-\cdot)]^{3-}$ is 76%. On the other hand, it seems that the amount of reduced species generated during the photolysis increases as the pH increases, which can be rationally interpreted as follows. Despite that the H_2 evolution rate at pH = 6.2 is larger than that at pH = 7.5 (Fig. 8B), the maximum concentration of the reduced species at pH = 6.2 is only a half of that seen at pH = 7.5. This simply suggests that the photoreaction populating the reduced species competes with the thermal process depopulating the reduced species. In other words, change in the maximum concentration of the reduced species reached during these two reactions (i.e., formation and consumption reactions) can be induced by the variation in the ratio of the formation and consumption reaction rates.

In order to observe the thermal HER driven by these one-electron-reduced species according to eqs. 9-11, the H_2 evolution that proceeds after stopping the photoirradiation was examined at pH = 6.2. As shown in Fig. 11a, the absorption band derived from the reduced

species at 840 nm slowly decays over 1 h after the light-off action was made (see also Fig. S8). When the same event is monitored on the basis of the amount of H₂ evolved, a quite consistent response was observed (Fig. 11b), where the measurements were carried out by adopting the continuous Ar-flow method (see experimental section for detail) by setting the flow rate at 2 mL/min. Moreover, the thermal HER after the light-off action can be observed even when the solution, immediately after the light-off, is completely purged with Ar (100 mL/min for 10 min) prior to monitoring the H₂ evolved using the same Ar-flow method (2 mL/min). This confirms that the H₂ evolution curve observed in Fig. 11b is not an artifact due to the Ar-purging technique in our analysis. In addition to these observations, a similar photolysis experiment was carried out using a sealed reaction vessel containing 22 mL of the photolysis solution and having ca. 8 mL of the inner gas phase volume, which revealed that a quite similar thermal H₂ evolution behaviour can be observed by gas chromatography after the light-off action (Fig. S9). These confirm that the H₂ evolution from water is indeed driven by [PtCl(tctpyH^{-•})]²⁻ as a dark reaction (see eqs. 9-11). This is in sharp contrast with the stable character of PV^{+•} (i.e., one-electron-reduced form of PV²⁺), which does not drive the thermal HER (2PV^{+•} + 2H⁺ → 2PV²⁺ + H₂ does not take place).^{13c} Finally, we have to note that we cannot completely exclude photo-driven generation of the doubly reduced species [Pt^ICl(tctpyH_n^{-•})]⁽⁴⁻ⁿ⁾⁻ which might be formed via the Z-scheme envisioned for PV²⁺ (see Scheme 4).

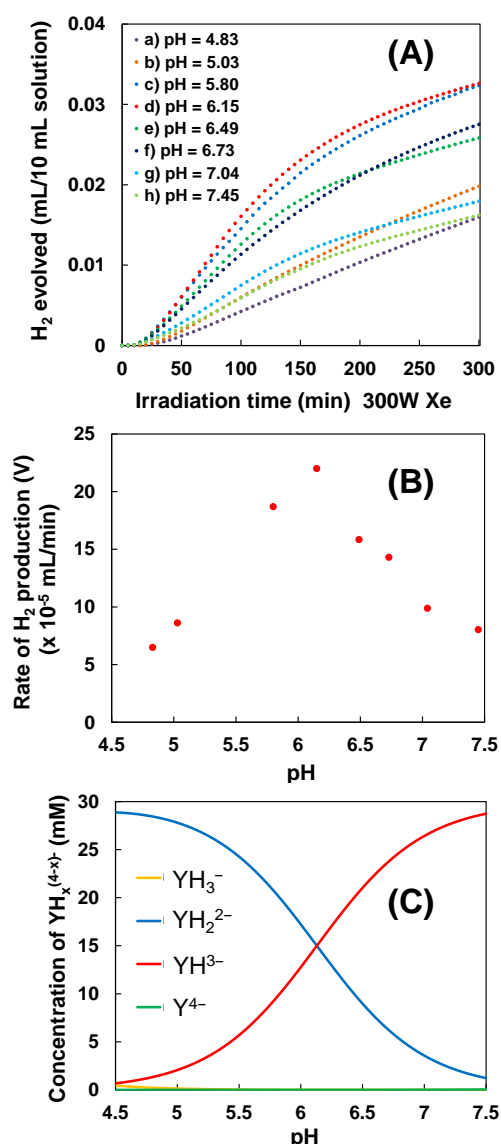


Fig. 8 (A) Photochemical H₂ production from an aqueous 0.1 mM Na₂[PtCl(tctpy)]•5H₂O solution (at 20 °C under Ar atmosphere) containing 0.1 M NaCl at a) pH = 4.83, b) pH = 5.03, c) pH = 5.80, d) pH = 6.15, e) pH = 6.49, f) pH = 6.73, g) pH = 7.04, or h) pH = 7.45, where pH was adjusted using a combination of Na₂[YH₂] and Na₃[YH] with a fixed total concentration (30 mM). (B) Plot of the maximum rate of H₂ production photocatalyzed by Na₂[PtCl(tctpy)]•5H₂O vs. pH, determined from the H₂ evolution curves in Fig. 8A. (C) Variation in the concentrations of YH_x^{(4-x)-} (x = 0, 1, 2, and 3) as a function of pH when the total EDTA concentration is 30 mM ([Y]_t = [YH₃⁻] + [YH₂²⁻] + [YH³⁻] + [Y⁴⁻] = 30 mM), where pK_a values employed are those in the literature (pK_{a2} = 2.67, pK_{a3} = 6.16, and pK_{a4} = 10.26).¹⁷

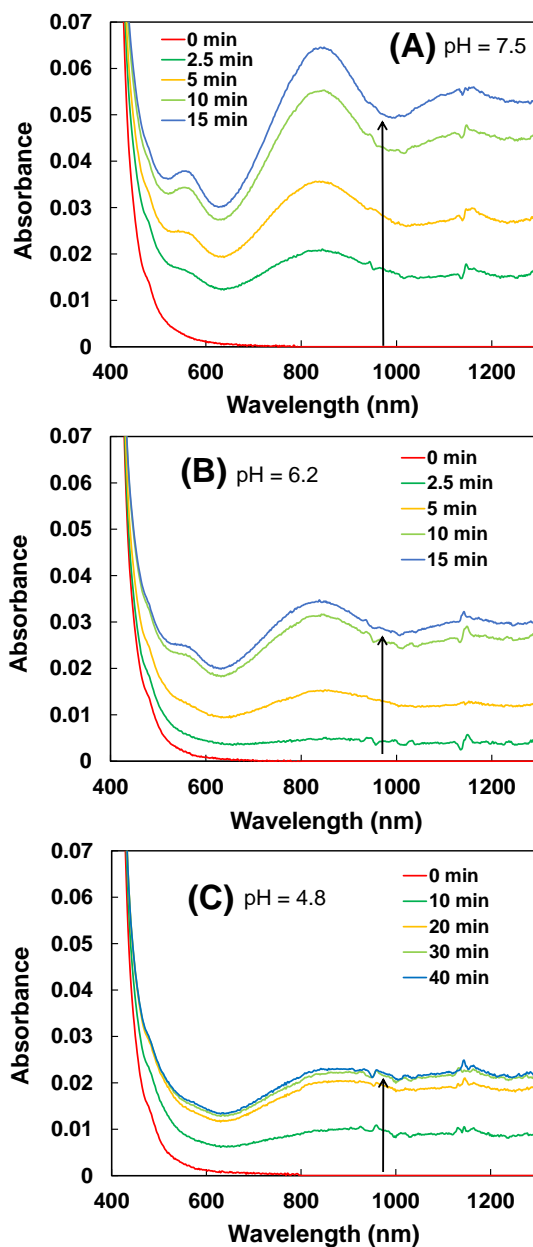


Fig. 9 Spectral changes during the photolysis (300 W Xe lamp, 400-800 nm) of an aqueous 0.1 mM $\text{Na}_2[\text{PtCl}(\text{tctpy})]\cdot 5\text{H}_2\text{O}$ solution (at 20 °C under Ar atmosphere) containing 0.1 M NaCl in the presence of (A) 1 mM $\text{Na}_2[\text{YH}_2]$, 29 mM $\text{Na}_3[\text{YH}]$, 16 mM NaH_2PO_4 , and 84 mM Na_2HPO_4 (pH = 7.5; 0.1 M phosphate buffer), (B) 15 mM $\text{Na}_2[\text{YH}_2]$ and 15 mM $\text{Na}_3[\text{YH}]$ (pH = 6.2), or (C) 29 mM $\text{Na}_2[\text{YH}_2]$ and 1 mM $\text{Na}_3[\text{YH}]$ (pH = 4.8). For A, additional use of phosphate somehow improved the reproducibility of the results. It should be also noted that spectral features of products are unaffected by the presence of phosphate, ruling out chloride replacement by phosphate donors. The blue line for each condition shows a spectrum affording maximum absorption during the course of photolysis.

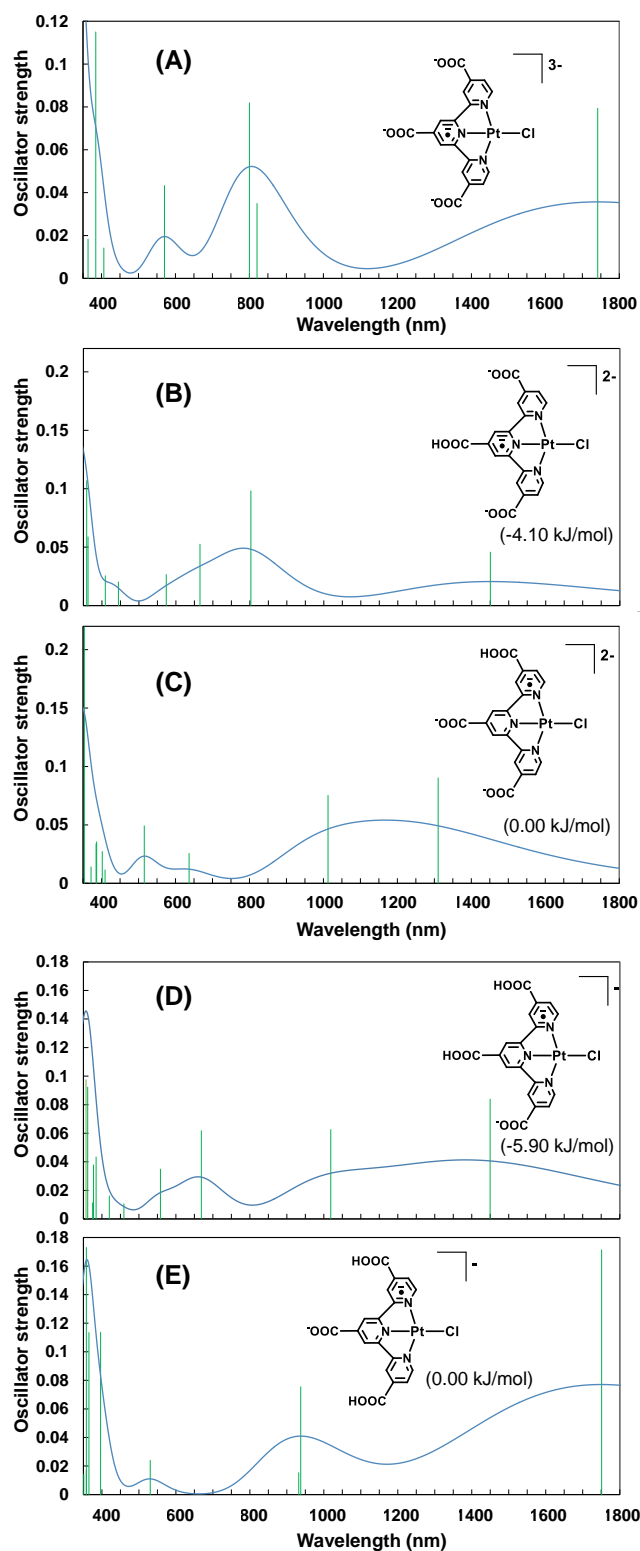


Fig. 10 TD-DFT simulated absorption spectra of five possible one-electron-reduced species; $[\text{PtCl}(\text{tctpy}^{\bullet})]^{3-}$ (A), $[\text{PtCl}(\text{tctpyH}^{\bullet})]^{2-}$ (B,C), and $[\text{PtCl}(\text{tctpyH}_2^{\bullet})]^{-}$ (D,E), where excitations are shown as vertical bars with heights equal to the oscillator strength (f). Relative energy among B and C, and that among D and E are shown with values in parentheses. Geometries optimized for each species are shown in Tables S5-S9, together with the spin

density distribution for each species. Each electronic transition is also summarized in Tables S10-S14.

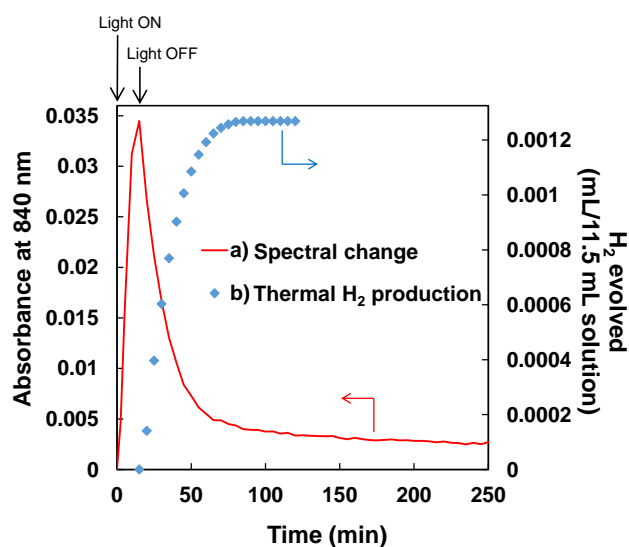


Fig. 11 Photoresponse properties examined for the photolysis of an aqueous $\text{Na}_2[\text{PtCl}(\text{tctpy})]\cdot 5\text{H}_2\text{O}$ solution in the presence of 0.1 M NaCl, 15 mM $\text{Na}_2[\text{YH}_2]$, and 15 mM $\text{Na}_3[\text{YH}]$ (pH = 6.2) at 20 °C under Ar atmosphere. The light-off action was made at 15 min after starting photoirradiation (300 W Xe lamp, 400-800 nm). a) The photoresponse observed by the change in absorbance at 840 nm. b) The dark reaction after the light-off action was separately monitored by detecting H_2 evolved using the continuous Ar-flow method (2 mL/min).

Ground state adduct formation of $[\text{PtCl}(\text{tctpy})]^{2-}$ with EDTA

As discussed above, the positively charged PHEMDs were shown to afford an ion-pair adduct required to enhance the reductive quenching of the triplet (Scheme 3), which was generally evidenced by observing their saturation kinetics in the photochemical H_2 evolution rate as a function of $[\text{EDTA}]$.^{12c,g,13} Our preliminary prediction avoided postulation of such an ion-pair adduct for $[\text{PtCl}(\text{tctpy})]^{2-}$ because of its dianionic character. Nevertheless, experiments in Fig. 12 clearly show that quite similar saturation behaviours are observed at both $\text{pH} = 5.0$ and 7.0 , where the major forms of EDTA in solution are YH_2^{2-} (93% abundance) and YH^{3-} (89% abundance), respectively. Quite similar saturation kinetics is observed at $\text{pH} = 6.2$ (see Fig. S11). Least-squares fitting analysis of these saturation curves provides apparent outer-sphere formation constants (K_{os} ; see Scheme 3) under these pH conditions; $K_{\text{os}} = 26, 59, \text{ and } 29 \text{ M}^{-1}$ at $\text{pH} = 5.0, 6.2, \text{ and } 7.0$, respectively. Importantly, the K_{os} is maximized at $\text{pH} = 6.2$ where the H_2 evolution rate is maximized (see Fig. 8B). Saturation is also seen when the H_2 evolution rate was examined as a function of the $[\text{PtCl}(\text{tctpy})]^{2-}$ concentration at a constant EDTA concentration (see Fig. S12). On the other hand, these adduct formation behaviours can be examined spectrophotometrically. The EDTA concentration dependence of absorption spectrum of $[\text{PtCl}(\text{tctpy})]^{2-}$ at $\text{pH} = 6.2$ ($[\text{YH}_2]^{2-} = [\text{YH}]^{3-}$) roughly shows that no essential change is induced in the coordination environment due to the variation in the total EDTA concentration (Fig. S13A). However,

careful analysis of absorbance changes at several wavelengths reveals that relatively small absorbance changes attributable to a shift of adduct formation equilibrium with $K_{os} = 59 \text{ M}^{-1}$ could be given upon changing the EDTA concentration with an isosbestic point located at 360 nm (Fig. S13). These results are consistent with our conclusion that this is not a ligand replacement equilibrium but corresponds to a relatively weak association between the two species. A possible interpretation may be that the positively charged ammonium groups may contribute to stable adduct formation between $[\text{PtCl}(\text{tctpy})]^{2-}$ and either YH_2^{2-} or YH^{3-} , as proposed in Scheme 5. Indeed, reports have shown that YH_2^{2-} and YH^{3-} exist primarily in their ammonium forms in aqueous media,¹⁸ which rationalizes the adduct formation proposed in Scheme 5. The reductive quenching of the photoexcited state of $[\text{PtCl}(\text{tctpy})]^{2-}$ (i.e., $[\text{PtCl}(\text{tctpy})]^{2-*}$) is likely to proceed only within such adducts because of the short-lived character of $[\text{PtCl}(\text{tctpy})]^{2-*}$ under these conditions (*vide supra*).

There are several factors affecting the apparent PHE activity of $[\text{PtCl}(\text{tctpy})]^{2-}$. First, the formal redox potential of EDTA ($E_{\text{ox,EDTA}}$) in aqueous media shows a cathodic shift upon an increase in pH. For instance, $E_{\text{ox,EDTA}}$ is reported as 0.32, 0.24, 0.17, and -0.17 V vs. SCE at pH = 2.1, 3.7, 4.8, and 9.2, respectively.¹⁹ Within the major adduct given at pH = 5.0 (adduct I in Scheme 5), reductive quenching becomes less favourable because of protonation at both nitrogen donors, which can also be rationalized due to the higher formal oxidation potential of EDTA, $E_{\text{ox,EDTA}}$, leading to a lower DF for the reductive quenching (DF =

$E_{1/2}([\text{PtCl}(\text{tctpy})]^{2-*}/[\text{PtCl}(\text{tctpy}^{-\bullet})]^{3-}) - E_{1/2}(\text{EDTA}^+/\text{EDTA})$. Moreover, the reductive quenching within adduct I is considered to proceed via a PCET process, in which ET from the nitrogen donor to the Pt^{III} atom in the $^3\text{MLCT}$ state must be accompanied by the proton transfer from a relevant nitrogen donor, e.g., to one of the adjacent carboxylate units of $[\text{Pt}^{\text{III}\rightarrow\text{II}}\text{Cl}(\text{tctpy}^{-\bullet})]^{(2\rightarrow3)-}$, where arrows show changes in oxidation state and charge that take place upon PCET. As for the reductive quenching within the major adduct at $\text{pH} = 7.0$ (adduct II in Scheme 5), ET from YH^{3-} to $[\text{PtCl}(\text{tctpy})]^{2-*}$ is much more favourable due to the presence of a non-protonated nitrogen donor, although the electrostatic stabilization is less favourable due to the smaller local positive charge given for YH^{3-} . It is quite reasonable to consider that the above-mentioned several competing effects could lead to the manifestation of the observed maximum rate in H_2 evolution. Thus far, we attempted to elucidate the adduct formation between $[\text{PtCl}(\text{tctpy})]^{2-}$ and EDTA simply based on ‘electrostatic models’. However, we cannot rule out involvement of other models, such as those supposing adducts stabilized with specific hydrogen-bonding interactions between the two species. We also avoid discussing the factors relevant to the rate-limiting processes in the subsequent steps after the reductive quenching takes place. Particularly, a possible PCET step, affording a hydride intermediate $[\text{Pt}^{\text{II}}\text{Cl}(\text{tctpyH}_n^{-\bullet})]^{(3-n)-} + \text{H}^+ \rightarrow [\text{Pt}^{\text{III}}\text{Cl}(\text{H})(\text{tctpyH}_n)]^{(2-n)-}$, may also contribute to the pH-dependent rate of H_2 evolution depicted in Fig. 8.

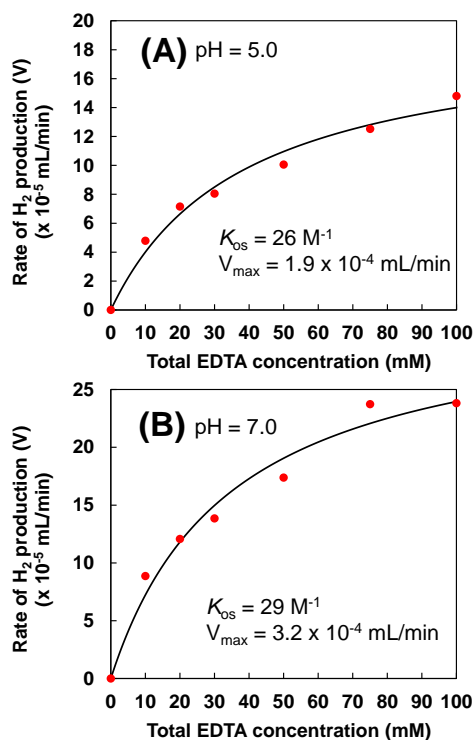
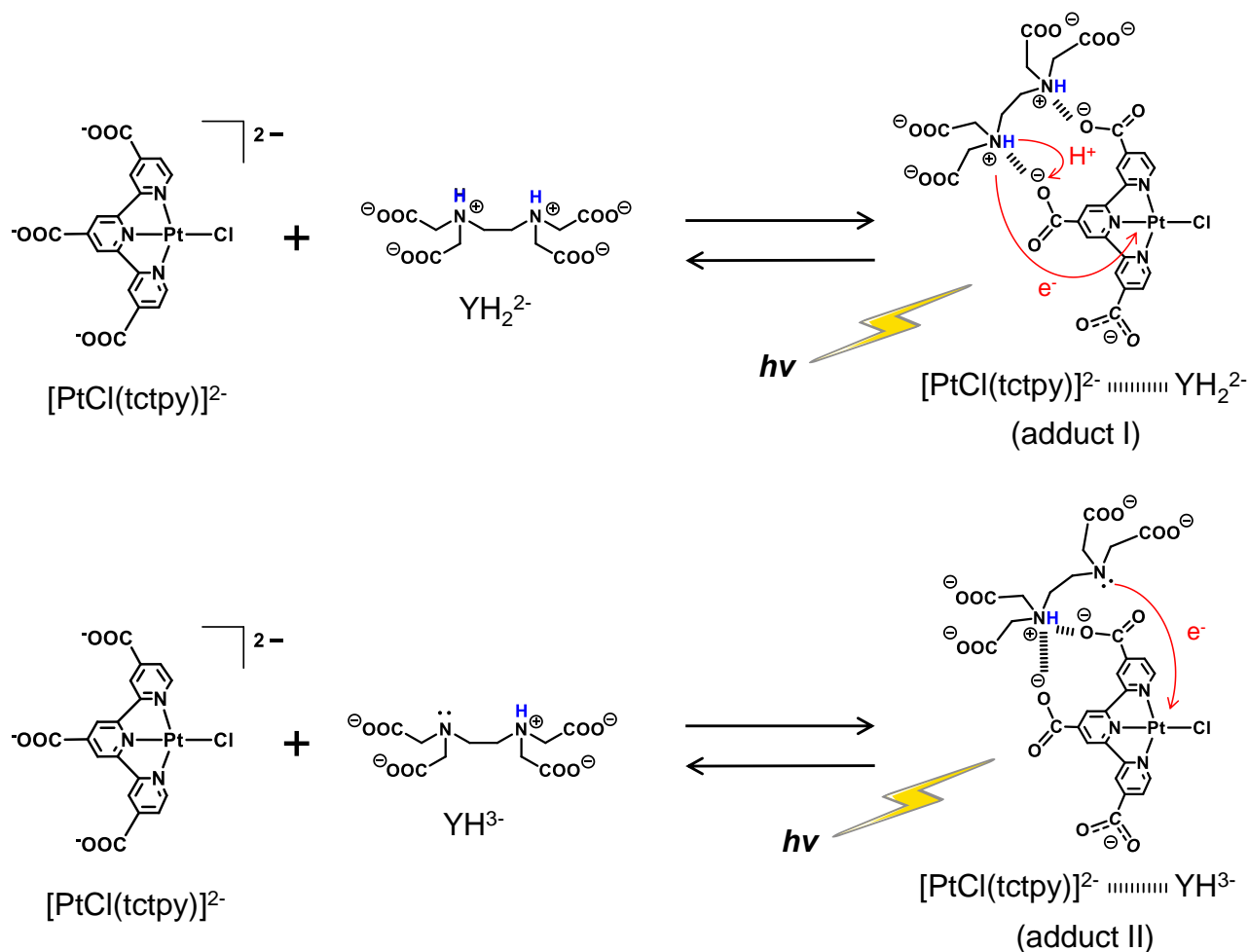


Fig. 12 The dependence of the maximum H₂ evolution rate on the EDTA concentration (0–100 mM) at a constant concentration of Na₂[PtCl(tctpy)]•5H₂O (0.1 mM) at (A) pH = 5.0 or (B) pH = 7.0, where the raw data are supplied as Fig. S10. Solid lines are calculated ones based on $V = V_{\max}[\text{EDTA}]_{\text{total}} / (K_{\text{os}}^{-1} + [\text{EDTA}]_{\text{total}})$.



Scheme 5 Possible structures for the adduct of $[\text{PtCl}(\text{tctpy})]^{2-}$ with YH_2^{2-} (adduct I) or YH^{3-} (adduct II), together with possible proton and electron transfer processes at the reductive quenching events.

Conclusions

We thus come to encounter an interesting Pt(II)-based molecular H₂ evolution catalyst whose basicity drastically increases upon forming the one-electron-reduced form, which allows us to demonstrate an important strategy to develop catalysts driving HER using a PCET process derived from the ligand geometry, which often lowers the reaction barriers of catalytic pathways. We also envision a special case in which two negatively charged species, that is, a photocatalyst and an electron donor, can form a weakly associated adduct which is essential to activate the photocatalyst's activity for H₂ evolution. Extended studies by adopting such strategies are now actively in progress.

Acknowledgements

This work was supported by a Grant-in-Aid for Scientific Research (B) (No. 24350029), a Grant-in-Aid for Scientific Research on Innovative Areas 'Coordination Programming' (No. 2107, 24108732), a Grant-in-Aid for Scientific Research on Innovative Areas 'Artificial Photosynthesis' (No. 2406, 24107004), a Grant-in-Aid for Research Activity Start-up (No. 24850014), and a Grant-in-Aid for Young Scientists (B) (No. 25810042) from the Ministry of Education, Culture, Sports, Science, and Technology (MEXT) of Japan. This work was partly supported by Kyushu University Interdisciplinary Programs in Education and Projects in Research Development (P&P). This was also supported by the International Institute for

Carbon Neutral Energy Research (WPI-I2CNER), sponsored by the World Premier International Research Center Initiative (WPI), MEXT, Japan.

Experimental Section

Materials

K_2PtCl_4 was purchased from Tanaka Kikinzoku Kogyo. All solvents and reagents were of the highest qualities available and were used as received without further purification. The ligand $(\text{tctpyH}_3)^{20}$ and $[\text{PtCl}(\text{tpy})]\text{Cl}\cdot 2\text{H}_2\text{O}^{21}$ were synthesized as previously described.

Synthesis of $\text{Na}_2[\text{PtCl}(\text{tctpy})]\cdot 5\text{H}_2\text{O}$

The ligand tctpyH_3 (0.331 g, 0.83 mmol) was dissolved in aqueous media by adding water and aqueous 0.1 M NaOH, while the pH was kept below 8, and the total volume of the solution reached ca. 35 mL at the end. To the solution were added K_2PtCl_4 (0.342g, 0.83 mmol) and NaCl (0.19 g, 3.3 mmol) followed by refluxing for 2 d. After cooling down to room temperature, the solution was filtered for the removal of insoluble materials if any. The pH of the filtrate was then adjusted to 3 using an aqueous 0.1 M HCl solution. The resulting green precipitate was collected by filtration, and washed with a minimum amount of water

and acetone (3 times for each solvent). The solid was then dissolved in an aqueous solution (100 mL) containing NaHCO_3 (0.1 M) and NaCl (1 M), followed by adding a large excess of methanol (900 mL). The orange powder deposited was collected by filtration, washed with cold methanol (3 times), and then dried in vacuo. Yield: 0.531 g (88%, 0.73 mmol). Anal. Calcd for $\text{C}_{18}\text{H}_{18}\text{N}_3\text{O}_{11}\text{Na}_2\text{ClPt}$: C, 29.66; H, 2.49; N, 5.77. Found: C, 29.51; H, 2.21; N, 5.64. ^1H NMR (methanol- d_4 /trimethylsilane, ppm): δ 9.14 (d, $J = 5.4$ Hz, 2H), 8.80–8.77 (m, 4H), 8.19 (d, $J = 5.4$ Hz, 2H).

Measurements

UV-vis spectra were recorded on Shimadzu UV-2600 and UV-3600 spectrophotometers. ^1H NMR spectra were acquired on a JEOL JNM-ESA 600 spectrometer. Luminescence spectra were recorded on a Shimadzu RF5300PC spectrofluorophotometer. Emission decays were recorded on a HORIBA FluoroCube 3000USKU, where the excitation source was a diode laser (374 nm) (HORIBA N-375L). Cyclic and square wave voltammograms were recorded on an ALS 602DKM electrochemical analyzer (BAS). For the experiments using dry dmf media, a platinum working electrode, a platinum wire counter electrode, and a Ag/Ag^+ reference electrode (ca. 0.25 V vs. SCE) were used, where TBAP (0.1 M) was used as a supporting electrolyte. The potentials were corrected by employing the ferrocene/ferrocenium (Fc/Fc^+) couple as an internal standard, in which the Fc/Fc^+ couple was considered to be 0.310 V vs. SCE. For the measurements

using aqueous media, a glassy carbon working electrode, a platinum wire counter electrode, and a saturated calomel reference electrode (SCE; 0.241 V vs. NHE) were employed, where KCl (0.1 M) was used as a supporting electrolyte. Photochemical hydrogen evolution experiments were carried out using the automated system developed in our group, as described elsewhere.^{5b,11} These experiments adopted a continuous Ar-flow method by setting the flow rate at 10 mL/min, unless otherwise noted. The photoirradiation was carried out by an ILC Technology CERMAX LX-300 300 W Xe lamp equipped with a CM-1 cold mirror which reflects lights in the range of $400 < \lambda < 800$ nm. DLS experiments were carried out using an Otsuka Electronics ELSZ-2PS particle analyzer equipped with a diode laser (660 nm). The pH measurements were performed using an HM-25R pH meter (DKK-TOA).

DFT calculations

The geometries of model structures were optimized at the M06 level²² of DFT using the LanL2DZ basis set²³ for Pt and the 6-31+G(d,p) basis set for H, C, N, O, and Cl, where the contribution of water solvation was also taken into account using the polarizable continuum model (PCM) method²⁴ implemented in Gaussian 09.²⁵ The LanL2DZ basis set uses relativistic effective core potentials (RECP) for Pt to account for the scalar relativistic effects of the inner 60 core electrons ($[\text{Kr}]4d^{10}4f^{14}$). Figures were made using GaussView 5.09.²⁶ Excited states were calculated by TD-DFT²⁷ as implemented in Gaussian 09.²⁵ These calculations employed the

hybrid M06 functional along with the basis sets described above. At least 300 excited states were calculated for each system. The calculated transitions were replaced by a Gaussian broadening function with a full width at half maximum height of 0.2 eV to simulate the electronic transition spectrum.

Notes and references

Electronic Supplementary Information (ESI) available: Figs. S1–S13 and Tables S1-S14. See

DOI: 10.1039/b000000x/

- 1 a) A. J. Esswein and D. G. Nocera, *Chem. Rev.*, 2007, **107**, 4022; b) V. Artero, M. Chavarot–Kerlidou and M. Fontecave, *Angew. Chem. Int. Ed.*, 2011, **50**, 7238; c) M. Wang, L. Chen and L. Sun, *Energy Environ. Sci.*, 2012, **5**, 6763; d) V. Artero and M. Fontecave, *Chem. Soc. Rev.*, 2013, **42**, 2338; e) V. S. Thoi, Y. Sun, J. R. Long and C. J. Chang, *Chem. Soc. Rev.*, 2013, **42**, 2388; f) J. R. McKone, S. C. Marinescu, B. S. Brunschwig, J. R. Winkler and H. B. Gray, *Chem. Sci.*, 2014, **5**, 865; g) D. L. DuBois, *Inorg. Chem.*, 2014, **53**, 3935; h) V. Artero and J.-M. Saveant, *Energy Environ. Sci.*, 2014, **7**, 3808.
- 2 a) L. Duan, F. Bozoglian, S. Mandal, B. Stewart, T. Privalov, A. Llobet and L. Sun, *Nature Chem.*, 2012, **4**, 418; b) A. Kimoto, K. Yamauchi, M. Yoshida, S. Masaoka and K. Sakai,

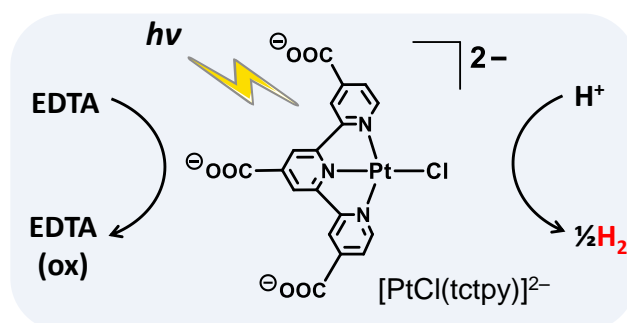
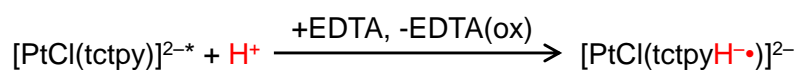
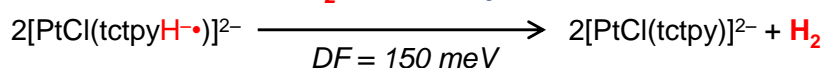
- Chem. Commun.*, 2012, **48**, 239; c) A. Singh and L. Spiccia, *Coord. Chem. Rev.*, 2013, **257**, 2607; d) M. Hirahara, A. Shoji and M. Yagi, *Eur. J. Inorg. Chem.*, 2014, 595; e) T. Kikuchi and K. Tanaka, *Eur. J. Inorg. Chem.*, 2014, 607; f) A. R. Parent and K. Sakai, *ChemSusChem*, 2014, **7**, 2070; g) M. Okamura and S. Masaoka, *Chem. Asian J.*, 2015, **10**, 306.
- 3 a) A. Kudo and Y. Miseki, *Chem. Soc. Rev.*, 2009, **38**, 253; b) K. Maeda and K. Domen, *J. Phys. Chem. Lett.*, 2010, **1**, 2655; c) A. Ryu, *J. Photochem. Photobiol. C*, 2010, **11**, 179; d) A. Kubacka, M. Fernández–García and G. Colón, *Chem. Rev.*, 2012, **112**, 1555; e) Y. Tachibana, L. Vayssieres and J. R. Durrant, *Nature Photonics*, 2012, **6**, 511.
- 4 a) K. Sakai and H. Ozawa, *Coord. Chem. Rev.*, 2007, **251**, 2753; b) H. Ozawa and K. Sakai, *Chem. Commun.*, 2011, **47**, 2227.
- 5 a) K. Sakai and K. Matsumoto, *J. Coord. Chem.*, 1988, **18**, 169; b) H. Ozawa, Y. Yokoyama, M. Haga and K. Sakai, *Dalton Trans.*, 2007, 1197; c) K. Yamauchi, S. Masaoka and K. Sakai, *J. Am. Chem. Soc.*, 2009, **131**, 8404; d) M. Ogawa, G. Ajayakumar, S. Masaoka, H.–B. Kraatz and K. Sakai, *Chem. Eur. J.*, 2011, **17**, 1148; e) K. Yamauchi, S. Masaoka and K. Sakai, *Dalton Trans.*, 2011, **40**, 12447.
- 6 T. M. Bockman and J. K. Kochi, *J. Org. Chem.*, 1990, **55**, 4127.
- 7 S. Tanaka, S. Masaoka, K. Yamauchi, M. Annaka and K. Sakai, *Dalton Trans.*, 2010, **39**, 11218.

- 8 K. Kawano, K. Yamauchi and K. Sakai, *Chem. Commun.*, 2014, **50**, 9872.
- 9 a) C. Baffert, V. Artero and M. Fontecave, *Inorg. Chem.*, 2007, **46**, 1817; b) X. Hu, B. S. Brunshwig and J. C. Peters, *J. Am. Chem. Soc.*, 2007, **129**, 8988; c) J. T. Muckerman and E. Fujita, *Chem. Commun.*, 2011, **47**, 12456.
- 10 a) M. L. Helm, M. P. Stewart, R. M. Bullock, M. R. DuBois and D. L. DuBois, *Science*, 2011, **333**, 863; b) W. Zhang, J. Hong, J. Zheng, Z. Huang, J. Zhou and R. Xu, *J. Am. Chem. Soc.*, 2011, **133**, 20680; c) Z. Han, L. Shen, W. W. Brennessel, P. L. Holland and R. Eisenberg, *J. Am. Chem. Soc.*, 2013, **135**, 14659; d) K. Yamauchi, *Bull. Jpn. Soc. Coord. Chem.*, 2013, **62**, 26.
- 11 H. Ozawa, M. Haga and K. Sakai, *J. Am. Chem. Soc.*, 2006, **128**, 4926.
- 12 a) H. Ozawa and K. Sakai, *Chem. Lett.*, 2007, **36**, 920; b) S. Masaoka, Y. Mukawa and K. Sakai, *Dalton Trans.*, 2010, **39**, 5868; c) H. Ozawa, M. Kobayashi, B. Balan, S. Masaoka and K. Sakai, *Chem. Asian J.*, 2010, **5**, 1860; d) M. Kobayashi, S. Masaoka and K. Sakai, *Molecules*, 2010, **15**, 4908; e) G. Ajayakumar, M. Kobayashi, S. Masaoka and K. Sakai, *Dalton Trans.*, 2011, **40**, 3955; f) M. Hirahara, S. Masaoka and K. Sakai, *Dalton Trans.*, 2011, **40**, 3967; g) C. V. Suneesh, B. Balan, H. Ozawa, Y. Nakamura, T. Katayama, M. Muramatsu, Y. Nagasawa, H. Miyasaka and K. Sakai, *Phys. Chem. Chem. Phys.*, 2014, **16**, 1607.

- 13 a) R. Okazaki, S. Masaoka and K. Sakai, *Dalton Trans.*, 2009, 6127; b) M. Kobayashi, S. Masaoka and K. Sakai, *Dalton Trans.*, 2012, **41**, 4903; c) M. Kobayashi, S. Masaoka and K. Sakai, *Angew. Chem. Int. Ed.*, 2012, **51**, 7431; d) K. Kitamoto and K. Sakai, *Angew. Chem. Int. Ed.*, 2014, **53**, 4618.
- 14 D. R. McMillin and J. J. Moore, *Coord. Chem. Rev.*, 2002, **229**, 113.
- 15 K. W. Jennette, J. T. Gill, J. A. Sadownik and S. J. Lippard, *J. Am. Chem. Soc.*, 1976, **98**, 6159.
- 16 J. F. Michalec, S. A. Bejune, D. G. Cuttell, G. C. Summerton, J. A. Gertenbach, J. S. Field, R. J. Haines and D. R. McMillin, *Inorg. Chem.*, 2001, **40**, 2193.
- 17 a) G. Schwarzenbach and H. Ackermann, *Helv. Chim. Acta*, 1947, **30**, 1798; b) D. C. Olson and D. W. Margerum, *J. Am. Chem. Soc.*, 1960, **82**, 5602.
- 18 a) K. Nakamoto, Y. Morimoto and A. E. Martell, *J. Am. Chem. Soc.*, 1963, **85**, 309; b) D. T. Sawyer and J. E. Tackett, *J. Am. Chem. Soc.*, 1963, **85**, 314; c) Y. Funaki, S. Harada and T. Yasunaga, *J. Phys. Chem.*, 1981, **85**, 693.
- 19 L. Meites and P. Zuman, *Electrochemical Data: Organic, Organometallic and Biochemical Substances Pt.1*, John Wiley & Sons Inc., 1975.
- 20 J. Dehaut, J. Husson and L. Guyard, *Green Chem.*, 2011, **13**, 3337.
- 21 G. Annibale, M. Brandolisio and B. Pitteri, *Polyhedron*, 1995, **14**, 451.

- 22 a) Y. Zhao and D. Truhlar, *Theor. Chem. Acc.*, 2008, **120**, 215; b) Y. Zhao and D. G. Truhlar, *J. Phys. Chem. A*, 2008, **112**, 1095; c) Y. Zhao and D. G. Truhlar, *Acc. Chem. Res.*, 2008, **41**, 157.
- 23 a) P. J. Hay and W. R. Wadt, *J. Chem. Phys.*, 1985, **82**, 270; b) W. R. Wadt and P. J. Hay, *J. Chem. Phys.*, 1985, **82**, 284; c) P. J. Hay and W. R. Wadt, *J. Chem. Phys.*, 1985, **82**, 299.
- 24 a) V. Barone, M. Cossi and J. Tomasi, *J. Comp. Chem.*, 1998, **19**, 404; b) M. Cossi, G. Scalmani, N. Rega and V. Barone, *J. Chem. Phys.*, 2002, **117**, 43; c) J. Tomasi, B. Mennucci and R. Cammi, *Chem. Rev.*, 2005, **105**, 2999.
- 25 M. J. Frisch et al., *Gaussian 09 Revision C.01*, Gaussian Inc., Wallingford CT, 2009.
- 26 GaussView 5.0.9, R. D. Dennington, T. A. Keith and J. M. Millam, *Semichem, Inc.*, Shawnee Mission, KS, 2009.
- 27 a) M. E. Casida, C. Jamorski, K. C. Casida and D. R. Salahub, *J. Chem. Phys.*, 1998, **108**, 4439; b) R. E. Stratmann, G. E. Scuseria and M. J. Frisch, *J. Chem. Phys.*, 1998, **109**, 8218; c) R. Bauernschmitt and R. Ahlrichs, *Chem. Phys. Lett.*, 1996, **256**, 454.

Table of contents

**Proton-coupled electron transfer (PCET)****Thermal H_2 evolution from water**

A 'negatively charged' PtCl(terpyridine) derivative was found to be the first example of Pt(II)-based molecular photocatalyst capable of driving H_2 evolution coupled with a PCET process at the ligand geometry.